Journal of the Korean Physical Society, Vol. 42, No. 3, March 2003, pp. 394∼400

Flux-Line Lattice and Surface Barrier in a Nb/Al Multilayer

Sang-Wook HAN*
Chemical Sciences Division, Lawrence Berkeley National Laboratory, California 94720, U.S.A.

(Received 16 December 2002)

The interaction of the flux line and the surface in a Nb/Al multilayer was studied with DC magnetization measurements for a magnetic field applied nearly parallel to the film surface and with a Gibbs free-energy calculation. Peaks were observed in the $M-H$ curves above the lower critical field, and a free-energy minimization calculation showed that the peak positions matched well with flux-line transitions of 1 row to 2 rows and 2 rows to 3 rows. When the field is applied at a small angle to the surface, an extra peak at small field, that was missed for a parallel field, was observed. With the free-energy calculation, we found that the extra peak corresponded to the lower critical field for flux-lines running parallel to the surface ($H_{c1\parallel}$). We point out that the flux lines in a thin-film superconductor follow the field applied with a sightly tilted angle to the surface for $H_{c1\perp} < H sin\theta$ and $H cos\theta < H_{c1\parallel}$, and rotate to be parallel to the surface at $H\cos\theta \simeq H_{c1\parallel}$.

PACS numbers: 74.25, 74.60, 74.78
Keywords: Vortex, Magnetization, Thin film, Lower critical field, Superconductor, Surface barrier, Free energy, Multilayer, Flux line

I. INTRODUCTION

In a type-II superconductor, magnetic vortices have been widely investigated theoretically as well as experimentally [1,2]. As a magnetic field is applied parallel to the surface of a superconducting film, the vortices not only feel a mutual repulsion but also the effects of the surfaces. The Bean-Livingston surface barriers [3,4] play an important role in the motion of vortices into and out of the superconductor. When the film thickness (t) is comparable to the London penetration length (λ_L), the interaction of flux lines with the surfaces strongly influence the flux-line orderings [5, 6]. Unusual peaks in a M-H curve above the lower critical field (H_{c1}) have been observed from superconducting films by using several different techniques, including electron tunneling [7], microwave absorption [8], resistivity [9], superconducting channel devices [10], SQUID magnetization [5, 11], torque magnetization [6], and vibrating reeds [12, 13]. Using a model calculation for minimizing the Gibbs free energy, Guimpel *et al.* [5] have suggested that the peaks could be due to a flux-line transition for spatial rearrangement. The idea of the free-energy minimization has been further developed by Brongersma *et al.* with Monte Carlo simulations [6]. The previous model calculations were applicable in only the thin-film limit where the film thickness was much smaller than the London penetration length. We applied the model for the free-energy minimization, without using an approximation, to the case of $t \simeq \lambda_L$ and found that the peaks agree well with the matching fields of flux-line transitions. Some aspects of this work have been previously investigated, our study improves on these by using careful measurements on a Nb/Al multilayer and free-energy calculations to show that the first peak observed at a tilted field is not due to a flux-line transition. From the free-energy calculation, we found that the extra peak position matched with the lower critical field for flux-lines running parallel to the surface. To our knowledge, we were the first to find that a peak in the $M-H$ curve above H_{c1} was not related to a flux-line matching field and that the peak could be missed for fields applied parallel to the surface. We also present the lower critical field models for a superconductor which has a smooth surface, comparing the model calculations to the cases of $YBa_2Cu_3O_{7-x}$ (YBCO) and Nb superconducting films.

In this paper, the model calculation for minimizing free energy is discussed in Sec. II, and the experimental details and the magnetization measurements are presented in Sec. III. We discuss the results in Sec. IV and summarize the main conclusions in Sec. V.

II. MODEL CALCULATION

As vortices run parallel to the surface of a superconducting film, the vortices interact with the surface as well as other vortices. The total Gibbs free energy of a

*E-mail: swhan@lbl.gov

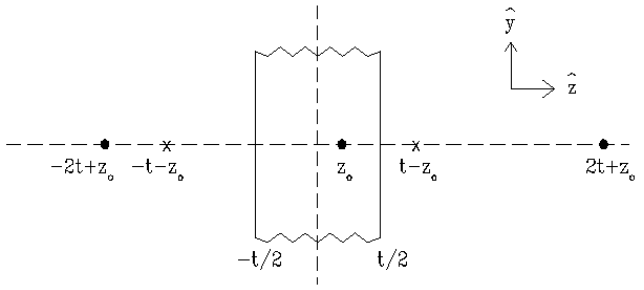

Fig. 1. Schematic diagram showing a vortex located at z_o and the series images generated by the two boundaries. Directions of the vortices are indicated by •(out) and x(in).

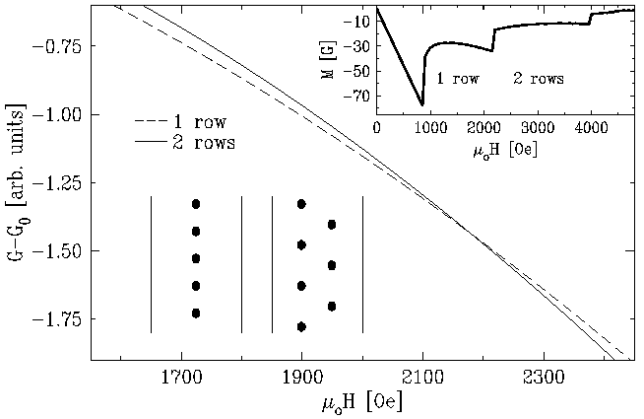

Fig. 2. Gibbs free energy as a function of the applied field with the vortices in 1 row (dashed line) and 2 rows (solid line). The inset at the lower left shows the configurations of the vortices, and the inset at the upper right shows the magnetization corresponding to the minimum free energy.

superconductor with N vortices is described as [4]

$$G = G_0 + \frac{1}{2\mu_o}\int_{V_S} dv\,\{\boldsymbol{\Phi}\cdot(2\boldsymbol{B}_L + \boldsymbol{B}_V - 2\mu_o\boldsymbol{H})\}\,, \quad (1)$$

where G_0 is the free energy for the system without vortices, μ_o is the permeability in vacuum, V_S is the volume of the superconductor, $\boldsymbol{\Phi}$ is the vorticity, $\boldsymbol{B}_L$ is the magnetic screening field, $\boldsymbol{B}_V$ is the magnetic field due to the vortices, and H is the external field. The magnetic field in a superconductor could be derived by solving the London equation:

$$\boldsymbol{B} + \lambda_L^2 \nabla\times\nabla\times\boldsymbol{B} = \boldsymbol{\Phi}. \quad (2)$$

For the Meissner region ($\boldsymbol{\Phi} = 0$), the magnetic field, which is a surface screening field, is taken to be

$$\boldsymbol{B}_L = \mu_o H \frac{\cosh(z/\lambda_L)}{\cosh(t/2\lambda_L)}\hat{x}, \quad (3)$$

where t is the total thickness of the superconducting film and the applied field is along the x-axis. If an isotropic and uniform superconductor is assumed, the vorticity with N vortices is

$$\boldsymbol{\Phi} = \Phi_o \sum_{k=0}^{k=N} \delta(\boldsymbol{r} - \boldsymbol{r}_k)\hat{x}, \quad (4)$$

where Φ_o is a flux quantum 2.067×10^9 G Å^2, $\boldsymbol{r}_k$ is the location of the kth vortex, and the vortices are oriented along the x-axis. For a single vortex ($\boldsymbol{\Phi}_o = \delta(\boldsymbol{r} - \boldsymbol{r}_o)$) in the superconductor, the magnetic field due to the vortex is

$$\boldsymbol{B}_V = \frac{\Phi_o}{2\pi\lambda_L^2} K_0\left(\frac{|\boldsymbol{r} - \boldsymbol{r_o}|}{\lambda_L}\right)\hat{x}, \quad (5)$$

where K_0 is a modified Bessel function of the zeroth order. A thin film has two boundaries, and the total magnetic field ($\boldsymbol{B}_L + \boldsymbol{B}_V$) should satisfy for the boundary condition, so $\boldsymbol{B}_V$ should vanish at the surfaces. We employ image vortices to solve this boundary problem, as shown in Fig. 1. The local magnetic field due to the vortex and its images can be described as

$$\boldsymbol{B}_V = \frac{\Phi_o}{2\pi\lambda_L^2}\sum_{n=-\infty}^{n=\infty}(-1)^n K_0\left(\frac{\sqrt{(z - nt - (-1)^n z_o)^2 + (y - y_o)^2}}{\lambda_L}\right)\hat{x}, \quad (6)$$

where $n = 0$ is for a real vortex and the other terms are for the images. With the same idea for a single vortex, the magnetic field at r (y,z) due to N vortices is

$$\boldsymbol{B}_V = \frac{\Phi_o}{2\pi\lambda_L^2}\sum_{k=-N/2}^{k=N/2}\sum_{n=-\infty}^{n=\infty}(-1)^n K_0\left(\frac{\sqrt{(z - nt - (-1)^n z_k)^2 + (y - y_k)^2)}}{\lambda_L}\right)\hat{x}. \quad (7)$$

The total free energy of a thin-film superconductor with N vortices can be obtained from Eq. (1) by substituting Eqs. (3), (4), and (7) for $\boldsymbol{B}_L$, $\boldsymbol{\Phi}$, and $\boldsymbol{B}_V$, respectively. In simplifying the free-energy calculation, previous studies [6, 14] have used an approximation for $\boldsymbol{B}_V$ which is valid only in the limit of $\lambda_L \gg t$. Since this approximation is not applicable for $\lambda_L < t$, we use Eq. (7) where we count term by term in the summation. With a London penetration length of 1800 Å and a *coherence length* (ξ) of 113 Å (these numbers will be discussed

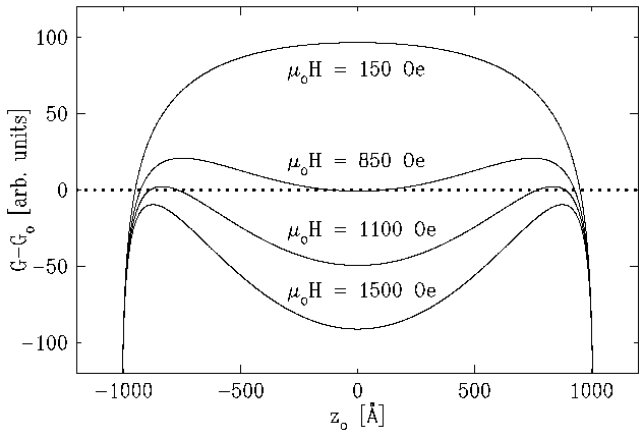

Fig. 3. Gibbs free energies as a function of the vortex position at different applied fields.

later), the free energy was calculated for increasing external field, as shown in Fig. 2. We assumed that the magnetic field within the core of the vortex was uniform with the same value at z = $z_k \pm \xi$. This assumption is valid for a large value of the Ginzburg-Landau parameter ($\lambda_L(T)/\xi(T)$), and most type-II superconductors satisfy this condition. In the calculations, only the density of vortices was varied for minimizing the free energy with the positions of the vortex rows fixed, such that z = 0 is 1 row, z = -$t/6$ and $t/6$ are two rows, and so on. When the applied field is 850 Oe, the superconductor allows vortex entrance to decrease the free energy of the system, and the vortices stay in the middle line of the film until the applied field reaches 2200 Oe. For μ_oH > 2200 Oe, the energy for two rows of vortices is smaller than that for the one-row configuration. The 2 → 3 row transition occurred at 3900 Oe. The inset shows the magnetization corresponding to the minimum free energy. This free-energy calculation with vortices was made under an equilibrium condition where vortices could enter the superconductor whenever the system needed vortices [15]. For a superconductor with smooth surfaces, the Bean-Livingston surface barrier prevents vortex entrance so that the lower critical field may be different from the one for the equilibrium state.

With the same free-energy model, we could also calculate the lower critical field ($H_{c1\|}$) with the surface barrier included. For a single vortex ($\mathbf{\Phi} = \Phi_o\delta(z-z_o)\delta(y-y_o)\hat{x}$), the total magnetic field was obtained by summing Eqs. (3) and (6). If the total magnetic field is put into Eq. (1), the free energy is

$$G = G_0 + \Phi_o\mu_o H\left(\frac{\cosh(z_o/\lambda_L)}{\cosh(t/2\lambda_L)} - 1\right) + \frac{\Phi_o^2}{4\pi\lambda_L^2}\left\{\sum_{n=-\infty}^{n=\infty}(-1)^n K_0\left(\frac{|(z_o - nt - (-1)^n z_o)|}{\lambda_L}\right)\right\}, \quad (8)$$

where the vortex position is z_o. The free energy depends on the vortex position and the applied field, as shown in Fig. 3. The lower critical field, $\mu_o H_{c1}$ ($\Phi_o/(4\pi\lambda_L^2)K_0(\xi/\lambda_L)$), for a bulk superconductor is calculated to be 150 Oe with λ_L = 1800 Å and ξ = 113 Å. The calculation indicates that a vortex cannot enter the superconductor at a field of 150 Oe. When the free energy is zero, the system is at equilibrium. For our system, the equilibrium state occurs at the applied field of 850 Oe when the vortex is located in the middle of the film. If no surface barrier exists, a vortex can enter the superconductor at the field for the equilibrium condition. However, this is not so for a superconductor with smooth surfaces, and the vortices cannot enter the superconductor until the surface barrier disappears near the surface. At μ_oH = 1100 Oe, the maximum value of the free energy is nearly zero, and the vortex position for the maximum is about a *coherence length* from the surface. That distance may be thought of as a required minimum length for a vortex to be nucleated near the surface. With this condition, G − G_0 = 0, $\mu_o H_{c1}$ is

$$\mu_o H_{c1} = \frac{\Phi_o}{4\pi\lambda_L^2}\frac{1}{1-\cosh(z_o/\lambda_L)/\cosh(t/2\lambda_L)}\left\{K_0\left(\frac{\xi}{\lambda_L}\right) + \sum_{n=-\infty, n\neq 0}^{\infty}(-1)^n K_0\left(\frac{|[1-(-1)^n]z_o - nt|}{\lambda_L}\right)\right\}. \quad (9)$$

Using Eq. (9), three different lower critical fields can be derived. The lower critical field ($H_{c1\|}$) for a vortex running parallel to a smooth surface can be obtained using z_o =t/2 − ξ. Using z_o = 0 at the equilibrium condition, $H_{c1\|e}$ is obtained, and the H_{c1} for a bulk superconductor is derived from the thick limit ($t \to \infty$), assuming that

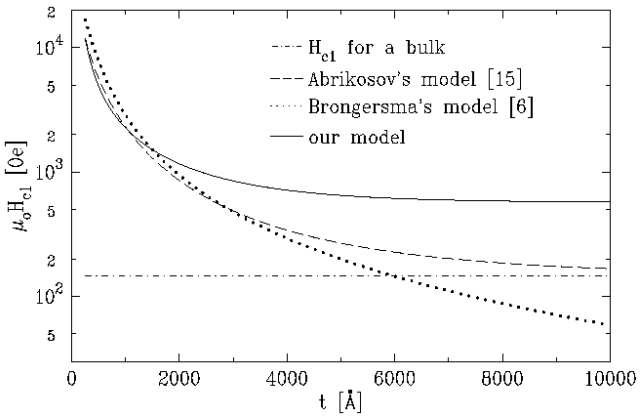

Fig. 4. Lower critical field calculated as a function of the film thickness with the different models.

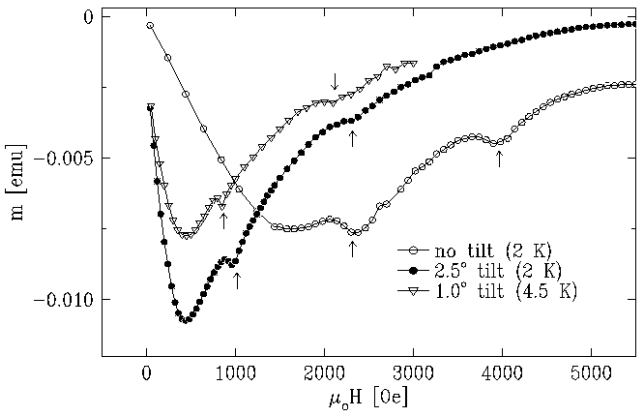

Fig. 5. Magnetic moments measured from a Nb/Al multilayer at 2 K and 4.5 K. Vertical arrows indicate the peaks. Data for 4.5 K were magnified by 5 times for clarity.

Table 1. Peak positions (Oe).

Tilt angle	Temperature (K)	1^{st}	2^{nd}
0.0°	2.0	2250	3900
2.5°	2.0	950	2250
1.0°	4.5	800	2050

the vortex is located away from the surfaces.

Several models have been studied for the lower critical field, as shown in Fig. 4. The H_{c1} for a bulk superconductor is from the Ginzburg-Landau theory [1,4]. However, it is not very useful for a thin-film superconductor because the theory does not effectively take into account the surface and the boundary effects. The lower critical field model for the equilibrium condition developed by Abrikosov [15] is very useful for a film superconductor with a large surface roughness that reduces the surface effect. As shown in Fig. 4, the lower critical field predicted by Abrikosov's model is eventually the same as the H_{c1} for a bulk superconductor for thick films. Brongersma *et al.* [6] also studied a model of the lower critical field in the thin-film limit ($\lambda_L \gg t$). The $H_{c1\|}$ predicted by our model is similar to that predicted by Abrikosov's model for a thin film. However, as the thickness gets larger, our model shows larger H_{c1} values than not only the prediction of the bulk model but also the prediction of Abrikosov's model. That is not too surprising because our model accounts for the surface effect independently of the thickness. The $H_{c1\|}$ model is valid for only the case of the parallel vortices entering a superconductor through a smooth surface instead of being nucleated in the middle of the superconductor.

III. MEASUREMENT AND RESULTS

The details of the preparations and characterizations of the multilayered specimen, Nb/[Nb(72 Å)/Al(20 Å)] $\times$ 20, are described elsewhere [16]. Glancing incident X-ray reflectivity measurements showed a well-structured multilayer with a total thickness of 2020 Å. The London penetration length was determined to be 1800 $\pm$ 200 Å by using spin-polarized neutron reflectivity. For the magnetization measurements, the samples were mounted on an extended sample holder placed in a cryostat so that the film surface was nearly parallel to the applied field of the SQUID magnetometer. The sample was zero-field cooled. Figure 5 shows ascending-field magnetic moments measured from the multilayer at 2 and 4.5 K. The magnetization reveals small peaks (indicated by vertical arrows). The peak positions are summarized in Table 1. The first peak was observed at a tilted field of ∼950 Oe. However, the first peak is missing for the no-tilt field under 2 K.

In order to identify the peaks, we compare the peak positions and the flux-line transition fields discussed in Sec. II. For the free-energy minimization calculation, two characteristic lengths, λ_L and ξ, are required. From the magnetization measurement for the field with no tilt, shown in Fig. 5, $\mu_o H_{c1\|}$ is 1100 $\pm$ 100 Oe. With the measured lower critical field ($H_{c1\|}$) and Eq. (9), ξ is ∼113 Å. The flux-line transition fields with λ_L = 1800 Å and ξ = 113 Å were determined, as shown in Fig. 2. From the calculations, it is clear that the first flux-line transition occurs around 2200 Oe, not near 950 Oe at which the first peak was observed in the SQUID magnetization measurement. Although the anisotropy of the Nb(72 Å)/Al(20 Å) multilayer should be taken into account for the free-energy calculation, Brongersma *et al.* [6] have shown that the anisotropy in a Nb(100 Å)/Cu(100 Å) multilayer is negligible in the free-energy calculation. Thus, our calculated result is probably not affected by the anisotropy effect very much.

Surprisingly, the measured first peak (950 Oe) at the tilted field is very comparable to the lower critical field for the equilibrium condition (850 Oe), as shown in Fig.

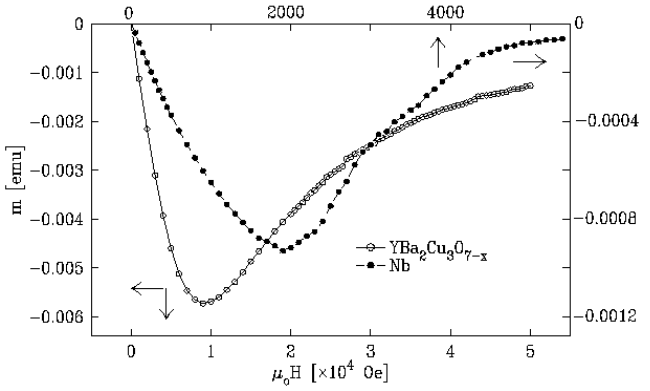

Fig. 6. Magnetic moments measured from 2500-Å-thick $YBa_2Cu_3O_{7-x}$ (open-circles) and 1440-Å-thick Nb (closed-circles) films. Please, be aware of the scales: left-bottom for YBCO and right-top for Nb.

2 inset, which implies that the first peak at the tilted field is not due to a flux-line transition, but is related to the lower critical field for vortices running parallel to the surface. At 4.5 K, the peak positions are observed at slightly smaller fields than they are at 2 K. This observation agrees with the SQUID magnetization study of a Nb/Si multilayer by S. M. Yusuf *et al.* [11], but contrasts with the torque magnetization measurements of S. H. Brongersma *et al.* for a Nb/Cu multilayer [6]. Based on the free-energy minimization calculation, the peak positions are determined by the characteristic lengths $\lambda_L(T)$ and $\xi(T)$. In order to understand the slight movement of the peak positions at different temperatures, further measurements of the temperature dependencies of $\lambda_L(T)$ and $\xi(T)$ with free-energy calculations are definitely necessary.

The results from our Nb/Al multilayer investigation were sufficient to show the interaction of the vortices and the surface. However, we wanted to cross-check the surface effect in other superconducting films. The magnetization measurements were carried out from a 2500-Å-thick YBCO film (high-T_c superconductor) and a 1370-Å-thick Nb film (conventional superconductor) under the same conditions as for the measurements on the Nb/Al multilayer. The magnetic moments are shown in Fig. 6. The preparations and characterizations of the YBCO [17] and the Nb [18] films are published elsewhere. It is quite interesting that we did not observe any peak from the films although Hünnekes *et al.* [12] by using internal friction measurements reported the observation of flux-line motions from a 2700-Å-thick YBCO film. There could be several possibilities for the lack of flux-line transitions in our sample; no transition exists, there is no sharp transition, the signal is too weak to be measured, and other possibilities. However, we can still apply the lower critical field models to the measurements. From the data in Fig. 6, the lower critical fields were determined to be 7000 ± 500 Oe for the YBCO film and 1100 ± 200 Oe for the Nb film. The lower critical fields for the three cases, Nb/Al multilayer ($t \simeq \lambda_L$), YBCO film ($t \simeq 2\lambda_L$), and Nb film ($t \simeq 3\lambda_L$), were calculated with different models and compared with the measurements, as shown in Table 2. The characteristic lengths were taken from previous studies [1,18–20]. The calculations show that Abrikosov's and Brongersma's models agree with only the Nb case because Abrikosov's model is not applicable for a superconductor with a smooth surface and Brongersma's model is limited to thin films ($t < \lambda_L$). Only our model agrees well with the measurements from all three superconducting films. From the free-energy calculation for the Nb film (not shown here), we found that the surface effect was negligible because of a relatively large vortex core size ($\xi \simeq 250$ Å).

IV. DISCUSSION

Using the free-energy calculation, we confirmed that the second and third peaks correspond to flux-line transitions and that the first peak is related to the parallel lower critical field ($H_{c1\|e}$) for the equilibrium condition. A sudden change of vortex density for a spatial rearrangement at a matching field can explain the peaks in the $M - H$ curve, as shown in the inset at Fig. 2. However, one might question whether the vortex rotation could create the peak because the rotation angle is small, only a few degrees. We have a mechanism for the vortex rotation. It is well known that vortices can enter a thin-film superconductor at a small field when the field is applied perpendicular to the surface [4]. For a tilted field of $Hsin\theta > H_{c1\perp}$, the vortices can enter the superconductor with help from the perpendicular component of the external field and run along the applied field due to the dragging force produced by the external field [21]. However, the vortices cannot run parallel to the film surface because the free energy of the system prevents the vortices from running parallel to the surface until $Hcos\theta > H_{c1\|e}$. At $Hcos\theta \simeq H_{c1\|e}$, the vortices are allowed to run parallel to the surface to reduce the free energy. At this point, the vortices existing nearly parallel to the surface are slightly rotated to be parallel to the surface.

In this scenario, the magnetization might change a small amount because the maximum difference is $\Phi_o(1 - \cos 2.5^\circ)$ per vortex. However, we find that a large demagnetization effect enhances the change of the magnetization by more than two orders of magnitude, due to the vortex rotation [16, 18]. For $H_{c1\perp} < H\sin\theta$ and $Hcos\theta < H_{c1\|e}$, the perpendicular magnetic field due to vortices is $n\Phi_o sin\theta/(1 - N)$, where n is number of vortices per unit area and N is the demagnetization factor, which is 0.9986 ± 0.0011 for our sample geometry [18]. As the vortices rotate to become parallel to the surface, the perpendicular component of the magnetic field due to the vortices will vanish with the demagnetization. It is possible that some vortices are entering directly from

Table 2. Lower critical fields were calculated with different models described in the text. In the calculation, we used t = 2020 Å, λ_L = 1800 Å, and ξ = 113 Å for the Nb/Al multilayer, t = 2500 Å, λ_L = 1400 Å, and ξ = 16 Å for the YBCO film, and t = 1370 Å, λ_L = 490 Å, and ξ = 250 Å for the Nb film.

Specimen	H_{c1} for a bulk	Abrikosov's [15]	Brongersma's [6]	our model	measured $\mu_o H_{c1\parallel}$
Nb/Al multilayer	147 Oe	850 Oe	935 Oe	1100 Oe	1100 ± 100 Oe
YBCO film	380 Oe	1198 Oe	1051 Oe	7197 Oe	7000 ± 500 Oe
Nb film	622 Oe	1056 Oe	1193 Oe	1005 Oe	1000 ± 200 Oe

outside instead of rotating at $H = H_{c1\parallel e}$. However, vortex entrance from the outside only cannot generate the observed peak because the magnetic field due to vortices is positive for an ascending field, and vortex entrance will reduce the negative magnetization of the superconductor. This means that the peak should move in a direction opposite to that in Fig. 5 if the peak corresponds to vortex entrance from outside. A transition of flux lines from being parallel to being perpendicular to the surface has been observed in a Nb film for descending fields [18]. Based on the two systems, a Nb/Al multilayer and a Nb film, we might conclude that vortices could choose either direction, parallel or perpendicular, depending on the free energy, for a field applied nearly parallel to the surface.

Although previous studies and this work have been quite successful in understanding the vortex-surface interaction, macroscopic measurements for the study of the vortex distribution are limited because the distribution of vortices is predicted from measured peak positions and the model calculations. There are many unknown parameters which might prevent the observation of a peak. Furthermore, this study showed that a peak might not be related to a flux-line transition. In order to better understand the vortex-surface interaction, we need microscopic measurements to directly observe the vortex positions. Spin-polarized neutron reflectivity, which is sensitive to the spatial gradient of the magnetization in a film, might be a promising tool for such a vortex-surface interaction study [16,18,20].

V. CONCLUSIONS

The peak positions observed in the SQUID magnetization measured for a Nb/Al multilayer ($t \simeq \lambda_L$) were successfully predicted by using a free-energy minimization. These peaks correspond to flux-line transitions driven by the surface effect and the flux-line mutual interaction. Because the vortex-surface interaction is repulsive, vortices first stay in the middle of the multilayer and consecutively change to 2 rows, 3 rows and more rows as the field is increased. For a sample with the applied field tilted, a low-field peak in the magnetization was identified as corresponding to a lower critical field parallel to the surface, and the value of the transition field agreed well with the calculated value for the equilibrium state. The applied field drags the flux lines, and helps rotate the flux-lines running parallel to the surface. Demagnetization enhances the effect of flux-line rotation at $H = H_{c1\parallel e}$.

ACKNOWLEDGMENTS

The author (S-W. Han) is pleased to acknowledge very informative discussions with P. F. Miceli and G. P. Felcher, and to gratefully acknowledge the support from J. Farmer for the SQUID magnetization measurements.

REFERENCES

[1] G. Blatter, M. V. Feigel'man, V. B. Geshkenbein, A. I. Larkin and V. M. Vinokur, Rev. Mod. Phys. **66**, 1125 (1994).

[2] Sang Boo Nam, J. Korean Phys. Soc. **31**, 426 (1997); Hyeong-Jin Kim, W. N. Kang, Eun-Mi Choi, Kijoon H. P. Kim and Sung-Il Lee, J. Korean Phys. Soc. **40**, 416 (2002); Joonhyun Yeo and Myoung Kwan Ko, J. Korean Phys. Soc. **42**, 178 (2003).

[3] C. P. Bean and J. D. Livingston, Phys. Rev. Lett. **12**, 14 (1964).

[4] P. G. de Gennes, *Superconductivity of Metals and Alloys* (Addison-Wesley, New York, 1989); T. P. Orlando and K. A. Delin, *Foundations of Applied Superconductivity* (Addison-Wesley, New York, 1991).

[5] J. Guimpel, L. Civale, F. de la Cruz, J. M. Murduck and I. K. Schuller, Phys. Rev. B **38**, 2342 (1988).

[6] S. H. Brongersma, E. Verweij, N. J. Koeman, D. G. de Groot, R. Griessen and B. I. Ivlev, Phys. Rev. Lett. **71**, 2319 (1993).

[7] J. Sutton, Proc. Phys. Soc. **87**, 791 (1966).

[8] P. Monceau, D. Saint-James and G. Waysand, Phys. Rev. B **12**, 3673 (1975).

[9] T. Yamashita and L. Rinderer, J. Low Temp. Phys. **24**, 695 (1976); N. Ya. Fogel and V. G. Cherkasova, Physica B **107**, 291 (1981); P. Lobotka, I. Vávra, R. Senderák, D. Machajdík, M. Jergel, Š. Gaži, E. Rosseel, M. Baert, Y. Bruynseraede, M. Forsthuber and G. Hilscher, Physica C **299**, 231 (1994).

[10] A. Pruymboom, P. H. Kes, E. van der Drift and S. Radelaar, Phys. Rev. Lett. **60**, 1430 (1988).

[11] S. M. Yusuf, E. E. Fullerton, R. M. Osgood II and G. P. Felcher, J. Appl. Phys. **83**, 6801 (1998).

[12] G. Hünnekes, H. G. Bohn, W. Schilling and H. Schulz, Phys. Rev. Lett. **72**, 2271 (1994).
[13] M. Ziese P. Esquinazi, P. Wagner, H. Adrian, S. H. Brongersma and R. Griessen, Phys. Rev. B **53**, 8658 (1996).
[14] Gilson Carneiro, Phys. Rev. B **57**, 6077 (1998),
[15] A. A. Abrikosov, *Fundamentals of the Theory of Metals* (Elsevier Science Publisher, Amsterdam, 1988).
[16] S-W. Han, J. Farmer, P. F. Miceli, G. Felcher, R. Goyette, G. T. Kiehne and J. B. Ketterson (unpublished).
[17] S-W. Han, S. Tripathy, P. F. Miceli, K. Covington, E. Badica and L. H. Greene, accepted for publication in Jpn. J. Appl. Phys.
[18] S-W. Han, J. Farmer, P. F. Miceli, I. R. Roshchin and L. H. Greene, Phys. Rev. B **62**, 9784 (2000).
[19] G. P. Felcher, R. B. Lainbowitz, P. Chaudhari and S. S. P. Parkin, Physica B **156 & 157**, 867 (1989); V. Lauter-Pasyuk, H. J. Lauter, M. Lorenz, V. L. Aksenov and P. Leiderer, Physica B **267-268**, 149 (1999).
[20] S-W. Han, J. F. Ankner, H. Kaiser, E. Paraoanu, L. H. Greene and P. F. Miceli, Phys. Rev. B **59**, 14 692 (1999).
[21] H. F. Hess, C. A. Murray and J. V. Waszczak, Phys. Rev. B **69**, 2138 (1994); H. F. Hess, C. A. Murray and J. V. Waszczak, Phys. Rev. B **50**, 16528 (1994).